Korean J. Chem. Eng., 36(12), 2035-2046 (2019)
DOI: 10.1007/s11814-019-0391-y

pISSN: 0256-1115
eISSN: 1975-7220

Antibacterial dynamic membranes loaded by cephalexin/amine-functionalized SBA_15 for Pb(II) ions removal

Maryam Darzipour, Mohsen Jahanshahi, Majid Peyravi†, and Soodabeh Khalili

Department of Chemical Engineering, Babol Noshirvani University of Technology, Shariati Ave., Babol 47148-71167, Iran
(*Received 2 May 2019 • accepted 22 September 2019*)

Abstract−Novel antibacterial dynamic membranes loaded by cephalexin/amine functionalized SBA_15 were fabricated for heavy metal removal from aqueous solution. The mesoporous CPX/NH_2-SBA_15 nanocomposite was formed as a uniform adsorptive and hydrophilic layer on the ultrafiltration polymeric membrane (PVDF). The modified adsorbent and membranes were characterized by SEM, XRD, N2 adsorption-desorption analysis, FT-IR, TGA, DSC and contact angle. A number of qualitative (well diffusion, disk diffusion) antibacterial assays were conducted against gram-positive *S. aureus* and gram-negative *E. coli*. In addition, to evaluate its anti-biofouling performance, the model concentrated bacteria suspension in liquid medium was used as a feed solution. 100% bacteria mortality for certain concentration and suitable inhibition zones up to 3.5 cm were attained. An increment in the flux recovery from 55% (for UF) to 87% (for self-forming dynamic membrane (DM)) and 91% (for pre-coated DM) indicated that the dynamic layer improved the anti-biofouling property of the support membrane. High Pb(II) removal efficiency (99.8%) was achieved for the modified membrane during dynamic filtration test. CPX/NH_2/SBA-15 dynamic membrane showed higher Pb^{2+} rejection than SBA-15 dynamic membrane because of amine groups located on the adsorbent surface. In general, membranes provide good performance like better flux and rejection besides antibacterial and anti-biofouling behavior.

Keywords: Dynamic Membrane, CPX/NH_2-SBA_15 Nanocomposite, Heavy Metal Removal, Antibacterial Property, Anti-biofouling Behavior

INTRODUCTION

A wide variety of hazardous heavy metals in wastewater represent a major threat to the water ecosystem [1]. Among them, lead causes many illnesses in the brain, blood, kidney and neural systems [2]. Unconventional water resources including heavy metal ions are well contaminated with bacteria [3]. The co-existence of the microorganism with heavy metal is also established in the wastewaters like landfill leachate and tannery wastewater [4,5]. Water purification as a significant topic affects our environment and the overall process economy [6-9]. Several technologies, such as chemical precipitation, ion exchange, coagulation and flocculation, solvent extraction, adsorption and membrane filtration or a combination of them, have been employed to address this issue [1,10]. Among the existing methods of water treatment, membrane technology has attracted significant attention due to space saving, cost-effectiveness and easy to operate [11-13]. Although nanofiltration and reverse osmosis are able to remove heavy metal efficiently, these pressure-driven operations are more exposed to fouling phenomenon and totally require higher energy consumption when compared with MF and UF [14,15]. To increase the ability of high permeable pressure driven membrane for heavy metal removal efficiently and to limit the attachment of bacteria and the formation of biofilm on the membrane surface, dynamic membrane (DM) has been attracting significant attention [16]. Dynamic membrane has the dual function of adsorption and filtration in wastewater treatment. This modern idea of membrane formation can be provided by filtering water solution of inexpensive adsorbent on a porous support layer in situ [17]. After long time separation, when the membrane is fouled, a temporary formed top layer can be removed and the support should be fit to prepare a new dynamic layer deposited in the same way. It is easily cleaned with water backwashing or surface brushing. With the advantages of easy cleaning and low filtration resistance, DM seems to be good for wastewater treatment [18].

The dynamic layer plays the main role of the barrier in heavy metals removal. To choose appropriate material as dynamic layer for heavy metal ions adsorption, some conditions must be noticed: (a) the adsorbent must be chemically stable under adsorption conditions; (b) high specific surface areas with small pores are needed; (c) good contact should be established between the adsorption sites of adsorbent and the metal ions [19,20]. Mesoporous silica meet these conditions since they have a large surface area, narrow pore size distribution, stable structure, mechanical and chemical stability and plenty of Si-OH energetic linkages on the outer part of pore walls for well-modified surface property [21-23]. Among the mesoporous silica family, SBA-15 is the most popular. Since pore diameters can be simultaneously controlled in the synthesis, SBA-15 is selected as the favorable one [24,25]. To obtain better Pb^{2+} removal efficiency, some efforts have been dedicated to adsorbent functionalization. Various studies have revealed the excellent effect of introducing different types of amine groups on mesoporous silica surface to create a highly effective adsorbent for removing toxic metal ions [26]. To avoid strict membrane biofouling, antibacterial membranes are a further direction. The dynamic layer, including adsorption

†To whom correspondence should be addressed.
E-mail: majidpeyravi@nit.ac.ir
Copyright by The Korean Institute of Chemical Engineers.

material and antibacterial material, can reinforce the antibiofouling activity and adsorb contaminant in situ [27,28].

The aim of this study was to prepare a new antibacterial dynamic membrane with the dual function of heavy metals removal from aqueous solution and anti-biofouling characteristic. From this point of view, PVDF ultrafiltration membrane was hydroxylated to prepare a support and covered by antibacterial nanocomposite (CPX/NH_2-SBA_15) as dynamic layer. Regarding the use of antibiotics extensively for treatment of bacterial infections, cephalexin with excellent antimicrobial activity against both Gram-positive and Gram-negative bacteria was applied to aminated SBA_15. Lead nitrate was applied to provide the model wastewater, being as cation (Pb^{2+}) form in aqueous solution. The sole antibacterial property of the DM membranes was corroborated by good diffusion and diffusion disk experiments.

EXPERIMENTAL

1. Materials and Equipment Apparatus

Poly vinylidene fluoride (PVDF, Arkema France) was used as support membrane polymer in this work. Dimethylformamide (DMF), polyvinyl pyrrolidone (PVP), toluene, hydrochloric acid, sodium hydroxide, potassium permanganate and sodium sulfite and tetraethylorthosilicate (TEOS 98%) were purchased from Merck. Pluronic (P123), (3-Aminopropyl) triethoxysilane 99% (APTES) and lead(II) nitrate were obtained from Sigma Aldrich. Cephalexin monohydrate was obtained from Sari Antibiotics Company. Peptone water, agar (96%), yeast extract and glucose needed for bacteriological experiments were obtained from HIMEDIA. *Escherichia coli* and *Staphylococcus aureus* were purchased from Babol University of Medical Sciences.

2. Synthesis of CPX/NH_2-SBA_15

SBA-15 was synthesized by a method reported by Cheng et al [29]. SBA-15 samples were synthesized using triblock copolymer EO20-PO70EO20 (Pluronic P123) as the structure-directing agent and tetraethylorthosilicate (TEOS) as the silica source in acidic condition. In a typical synthesis, 4 g of P123 was dissolved in 130 mL mixture of deionized water and 2 M HCl solution which was stirred at 40 °C to get a homogeneous solution. 9 mL of TEOS was added dropwise to the solution under vigorous stirring. After being slowly stirred for 24 h at 40 °C, the mixed solution was aged in Teflon-lined autoclave at 100 °C for 48 h. The resulting material was collected by filtration, followed by washing with water and dried at 80 °C for 12 h. The surfactant was removed by calcination at 550 °C in the air for 6 h.

For amination, 1 g SBA-15 was suspended in 250 mL dried toluene. 0.5 gr APTES was added to the mixture and stirred under reflux for 24 h. Grafted material (NH_2-SBA_15) was collected by filtration under vacuum and washed with dried toluene. These samples were dried overnight in a vacuum oven at 40 °C [30].

For the cephalexin monohydrate (CPX) loading, 30 mg of the NH_2-SBA_15 were impregnated in aqueous solution with a CPX dosage of 1 g L^{-1}. The suspension was stirred vigorously for 24 h, finally, was centrifuged at 6,000 rpm for 10 min and washed three times with deionized water, followed by drying in a vacuum oven. To determine the loading percentage of CPX on NH_2-SBA_15, the supernatant was collected, then was obtained by measuring UV-Vis absorbance at 262 nm [31] then minus it from total cephalexin which we added; now we have the calculated CPX reacted with composite. The CPX loading percentage of the synthesized sample was calculated by using Eq. (1);

$$\text{CPX\%} = \frac{\text{The weight of loaded CPX (mg)}}{\text{The weight of } NH_2\text{-SBA_15}} * 100 \quad (1)$$

3. Preparation of Supporting Membrane

3-1. PVDF Hydroxylation Method

The pristine PVDF powder was first immersed in an alkaline solution of NaOH and $KMnO_4$ for at least 1 hr at 60 °C: (1 L deionized water need 20 gr NaOH (0.5 M) and 10.2 gr of $KMnO_4$ 1% weight percent), and then filtered and washed with deionized water. The white color of PVDF changed to violet. After that, this powder was submerged in acidic solution (pH=3.5) with Na_2SO_3 (1.2%) until the PVDF color changed to hoary. Finally, modified PVDF was washed with deionized water and dried [32].

3-2. Membrane Preparation

First, the PVDF powder was dried in an oven to remove trace gas and water for at least four hours. PVDF (16 wt%) and PVP (1 wt%) powder were dissolved in DMF to prepare casting solution by stirring at 40 °C. PVP was used as a pore former in the substrate. In fact, an increase in porosity can be attributed to affinity of non-solvent and PVP that varies the exchange rate between solvent and non-solvent during the phase separation process. The homogeneous solution was defoamed for 6 h. Homemade casting knife was used for casting solution on polyester non-woven fabric by the thickness of 100 micrometers. Then the glass plate was immersed in a coagulation bath (water) at room temperature. After film formation, the prepared membranes were stored in cleaned deionized water for at least one day to complete the phase inversion process [33].

4. Preparation of Dynamic Membranes

Considering the dynamic membrane formation process, two types of dynamic membranes were prepared: pre-coated DM and self-forming DM. A specified concentration of the adsorbent suspension (SBA_15 and CPX/NH_2-SBA_15) was prepared and filtered on the polymeric flat sheets sest up in the stainless steel dead-end module. The dynamic layer was filtered on the surface of the hydroxylated PVDF UF membrane as time passed.

Pre-coated SBA_15 or CPX/NH_2-SBA_15 DM was formed before the filtration of Pb^{2+} solution as follows: SBA_15 particles were first added into water to provide SBA_15 suspension with SBA_15 concentration of 1 g/L. Then the suspension was filtered by support polymeric membrane at a constant pressure of 3 bar. The filtration of SBA_15 suspension stopped at the permeate volume of 200 mL, and the sediment dose of SBA_15 on polymeric membrane surface was mathematically about 0.2 g. The same procedure was applied to prepare CPX/NH_2-SBA_15 pre-coated DMs.

Self-forming DM was formed within the filtration of heavy metals: SBA_15 particles were added directly into the water containing Pb^{2+} solution at SBA_15 concentration of 1 g/L. Then, the mixture solution was filtered on the support polymeric membrane. The filtration stopped at the permeate volume of 200 mL, and the sediment dose of SBA_15 on polymeric membrane surface was about

Table 1. Composition of various components in support membranes (weight percent) and dynamic layer material

Membrane name	Support membrane			Dynamic membrane	
	PVP	PVDF-OH	PVDF	CPX/NH_2-SBA_15	SBA_15
UF 1	1	0	16	-	-
UF 2	1	16	0	-	-
DM 1	1	16	0	-	×
DM 2	1	16	0	×	-

0.2 g theoretically. The same procedure was applied to prepare CPX/NH_2-SBA_15 self-forming DMs. The composition of the prepared supports and DM membranes is listed in Table 1.

5. Characterization Assay

Scanning electron microscopy (SEM) was applied for morphological study using an SNE45000M equipped at 30 kV. A thin layer of gold was sprayed on sample surfaces before observation. Presence of cephalexin particles was verified by EDX spectra at 30 KV. X-ray diffraction (XRD) analysis of the base sample (SBA_15) was carried out using the Cu anode in range 0.7-10 (low-angle) on X' Pert Pro model of Panalytical Company. The changes of functional groups in modified samples were characterized by FTIR (BFRL WQF - 510A, Germany) containing wavenumbers from 600 to 4,000 cm^{-1}. The specific surface area, pore volume and pore size of SBA_15, NH_2-SBA_15 and CPX/NH_2-SBA_15 were examined by N_2 adsorption-desorption isotherms with Belsorp mini equipped made in Japan at −196 °C (77 K). In this case, samples were degassed in vacuum at 100 °C for 12 h. To calculate the wrapped content of cephalexin in the adsorbent pores, a thermogravimetric analyzer (TGA, model: shimadzu50, Japan) was used. All samples were heated from 23 °C to 700 °C with a major heating rate of 10 °C/min. The thermal stability of the particles was taken by differential scanning calorimetry (model: DSC-400, Iran). The surface AFM photos of membranes and particles were taken by Nanosurf AFM (model: easyscan2 flex AFM, Swiss). AFM was used to investigate the size distribution of adsorbent and membrane pores. A contact angle measurement apparatus (OCA 15 plus, Dataphysics) was used to investigate the wettability of neat and hydroxylated PVDF UF membranes. The contact angle of water drop on membrane's surfaces was calculated by angle measuring software and CCD camera.

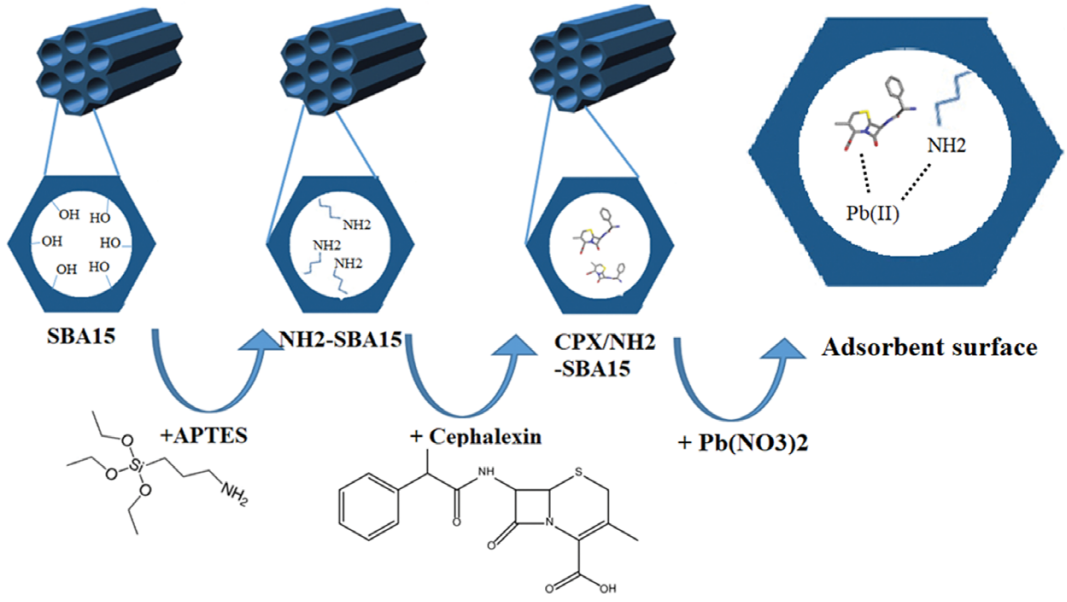
6. Performance Experiments

6-1. Adsorption Experiments

Pb(II) adsorption by synthesized materials was studied by batch operation in optimum condition understanding from previous studies. Lead solutions were prepared from $Pb(NO_3)_2$ with deionized water. Batch adsorption experiments were at 25 °C under natural pH conditions in a shaker incubator at 150 rpm for 1 h, using 20 mL of 200 ppm Pb(II) solutions and 0.1 g of the synthesized adsorbents. The results show the high adsorption capacity, 93.7%, 99.3% and 98.4% for SBA_15, NH_2-SBA_15 and CPX/NH_2-SBA_15, respectively. Scheme 1 shows a schematic of the nanocomposite synthesis process and Pb^{2+} adsorption.

6-2. Membrane Performance Experiments

The permeation properties of dynamic membranes were gauged by a laboratory-scale dead end system containing a cell with an effective area of 23.75 cm^2. The permeation flux and operating time were registered regularly. The permeation flux J (gr m^{-2} h^{-1}) was



Scheme 1. Synthesis of CPX/NH_2-SBA_15 and Pb^{2+} adsorption.

calculated with Eq. (2) [34]. The Pb^{2+} rejection efficiency was calculated according to Eq. (3).

$$J=m/A\Delta t \quad (2)$$

$$R\% = \frac{C_f - C_p}{C_f} * 100 \quad (3)$$

where m (gr) is the permeate mass, A (m^2) represents the membrane area, and Δt (h) denotes filtration time. C_f and C_p are the Pb^{2+} concentrations of the feed and permeate, respectively. Pb concentration was determined by atomic absorption spectroscopy (AAS). Normalized flux was obtained using the following expression:

$$\text{Normalized flux} = J/J_0 \quad (4)$$

where J (gr m^{-2} h^{-1}) is the permeate flux and J_0 is the pure water flux.

7. Antibacterial Experiments

7-1. Bacterial Growth

Bactericidal tests were done with gram-negative bacteria *E. coli* and gram-positive bacteria *S. aureus* in the culture medium. According to the manual, *E. coli* or *S. aureus* suspension was provided in nutrient broth cultures consisting of 5 g/L peptone water, 3 g/L yeast extract, 5 g/L glucose and distilled water which was autoclaved in advance. The strains were added into the flask of broth media in same, then set in the incubator shaker at 37 °C for 24 h to reach the log phase of the strains. For providing solid media, the nutrient media was completed with adding 15 g/L agar as a solidifying agent.

7-2. Disc Diffusion Method

Bacterial sensitivity to antibiotics was usually experimented with a disk diffusion test. The same experiment with nanocomposite laden disks was applied in this project [35]. A 10 mL suspension of nanocomposite (5 $mgmL^{-1}$) was sonicated, the laden filter papers were punched out to small uniform size disks (6 mm diameter). Then papers were immersed in the suspension. After preparation of agar cultures, a bacterial suspension (104 colonies forming unit (CFU)) was spread on the surface of agar plates uniformly before putting the disks on the center of each plate. The Petri dishes were incubated at 37 °C for 24 h; after that the mean diameter of the inhibition zone surrounding the disk was metered with calipers.

7-3. Well Diffusion Assay

The well diffusion assay was accomplished to check and discuss the qualitative analysis of antibacterial properties of antibiotics and nanocomposites [36]. 10^5 CFU/mL of each bacterial suspension was spread on the agar plates. Holes of 11mm size were dug in the agar plate, 10 mg of SBA_15, CPX/NH_2-SBA_15 and cephalexin were added to each hole. The plates were located in an incubator in the same condition. The zone of clearance was recorded.

8. Anti-biofouling Experiment

8-1. Bacterial Filtration

To evaluate the bio-fouling behavior of formed membranes, a concentrated suspension of bacteria was filtered into variant formed dynamic membranes [37]. The suspension of *E. coli* was determined to be very high (5.5×10^{17} CFU per milliliter) due to the biofouling to be obvious. Each part of the filtration device that was in contact with bacteria was washed and autoclaved before every test. Experiments were accomplished in the same condition at the ambient temperature. The permeation flux and operating time were registered regularly. To evaluate the biofouling-resistant capability of dynamic membranes, the flux recovery rate was measured by the following expression:

$$FR\% = \frac{J}{J_0} * 100 \quad (5)$$

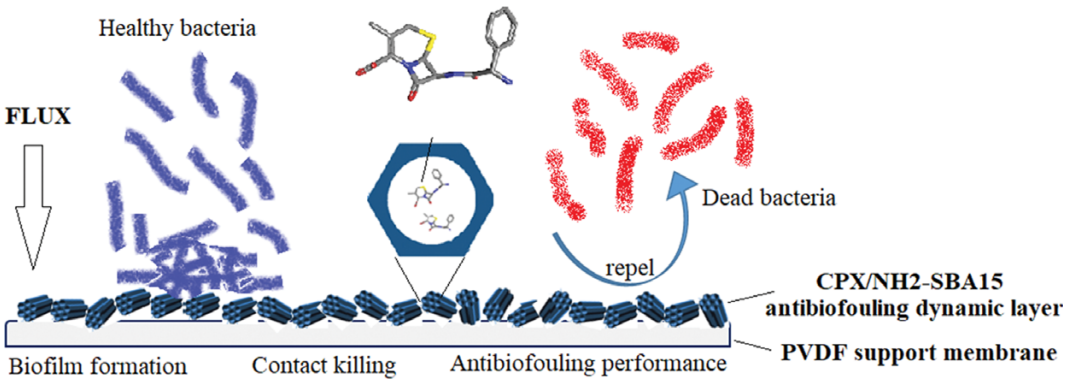
where J (gr m^{-2} h^{-1}) is the permeate flux of *E. coli* by the time and J_0 is the culture medium flux. Scheme 2 shows the antibiofouling property of antibacterial dynamic membrane against biofilm formation. Note that even a minimum amount of CPX/NH2-SBA_15 nanocomposite could inhibit and kill bacteria and hinder the biofilm formation.

RESULTS AND DISCUSSION

1. Characterization of SBA_15, NH_2-SBA_15 and CPX/NH_2-SBA_15

1-1. Scanning Electron Microscopy (SEM)

SBA-15 was synthesized in distinct morphologies containing fiber-like, doughnut-like and rope-like, which among them the last morphology is more desirable for adsorption [38]. Shahbazi et al. showed many ropelike domains with relatively uniform size of approximately 1 μm, which was in good agreement with the SBA-15 morphology [39]. As shown in Wang et al., SEM analysis, rod-like structure was clearly recognized from SBA-15, which means the successful preparation of SBA-15 [40]. In this research, the synthe-



Scheme 2. Antibiofouling performance of antibacterial DM.

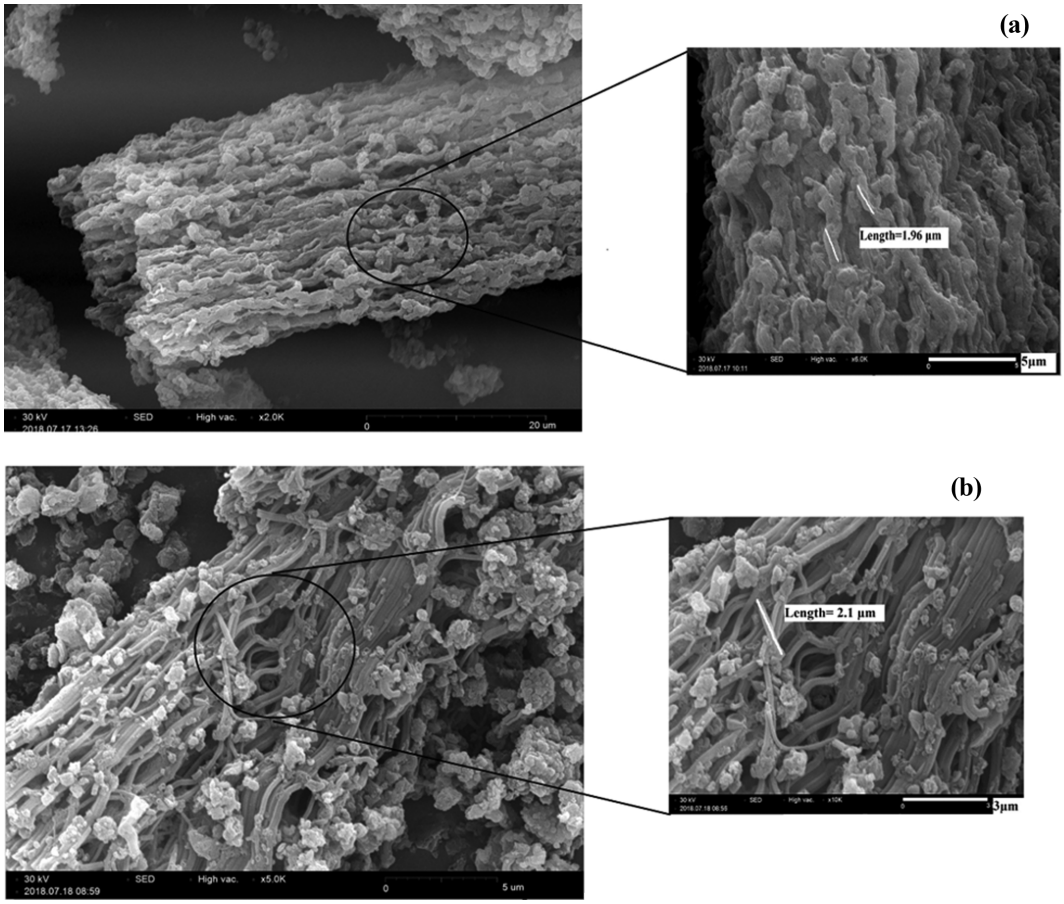


Fig. 1. SEM micrographs: (a) SBA_15, (b) CPX/NH_2-SBA_15.

sized SBA-15 represents a rope-like morphology with relative diameter of 100 nm and length of 2 μm as shown in Fig. 1(a). Fig. 1(b) shows the SBA-15 with cephalexin loading, which has similar morphology with SBA-15. It is obvious that functionalization and cephalexin loading had no effect on the particle morphology. The EDX results confirmed the presence of C, N and S elements in CPX/NH_2-SBA_15 (Fig. 2).

1-2. X-ray Diffraction

The low angle XRD pattern of SBA_15 based sample is shown in Fig. 3. As seen, the plot shows well-resolved characteristic peaks, which is related to a bi-dimensional p6mm hexagonal structure of the host SBA-15: an intense peak (100) at 2θ: 1.07 and two minor

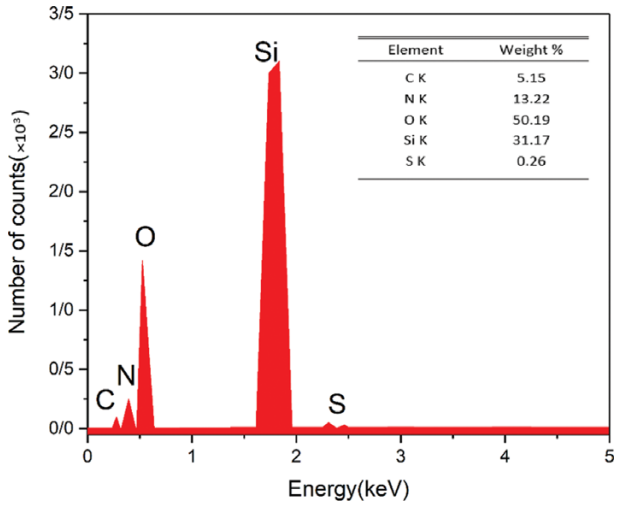


Fig. 2. EDX of CPX/NH_2-SBA_15.

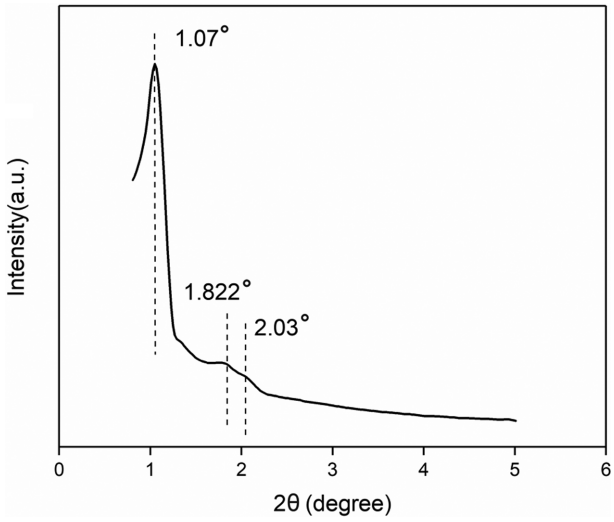


Fig. 3. XRD of SBA_15.

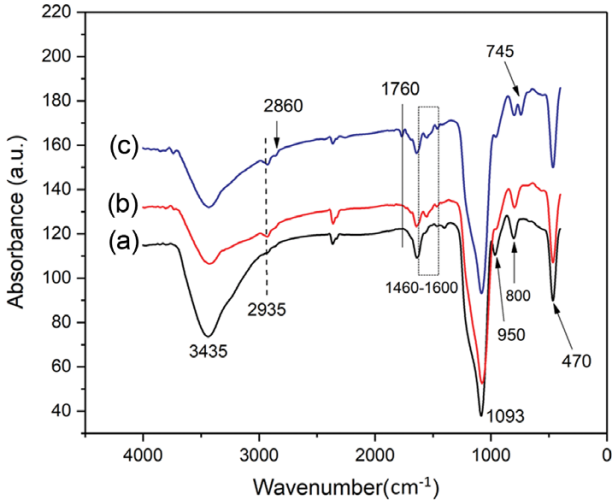


Fig. 4. FTIR Spectra: (a) SBA_15, (b) NH_2-SBA_15, (c) CPX/NH_2-SBA_15.

peaks (110 and 200) at about 2θ: 1.822 and 2.03 [41]. This result confirms the success of SBA-15 type of mesoporous silica synthesis.

1-3. FTIR Spectra

Fig. 4 displays the FT-IR spectra of unfunctionalized SBA-15 and provides evidence for APTES functionalization and cephalexin loading. The typical vibration peaks of SBA-15 (OH, 3,435 cm^{-1}; Si-O-Si, 1,093 and 800 cm^{-1}; Si-OH, 950 cm^{-1}; and Si-O, 470 cm^{-1}) were observed. Compared to the peak intensity in the SBA-15, the intensity of the Si-OH stretching vibration at 950 cm^{-1} in NH_2-SBA-15 decreased, which demonstrated that amine groups had occupied most of the Si-OH bends of SBA-15 [21]. In addition, the vibration peaks in the range of 1,460-1,600 cm^{-1} in the spectrum of NH_2-SBA-15 show the existence of the N-H bonding vibrations after the functionalization. Both symmetric and asymmetric stretching vibrations of C-H groups were identified at 2,860 and 2,935 cm^{-1} [42]. Therefore, these results confirm that aminopropyl groups are grafted on the inward surface of SBA-15 by reactions between OH groups and APTES. The characteristic bands apparent at 1,760 and 745 cm^{-1} are with respect to four-membered lactam carbonyl and C-S stretching vibrations, respectively [31]. As a result, it indicated that cephalexin was entrapped in NH_2-SBA_15 pores (Fig. 4(c)).

1-4. N2 Adsorption-desorption Isotherm

N2 adsorption/desorption isotherms of SBA-15, NH_2-SBA-15 and CPX/NH_2-SBA-15 are illustrated in Fig. 5. According to IUPAC classification, all three prepared samples demonstrate typical irreversible IV-type isotherms with an H1-type hysteresis loop that represents a general feature of mesoporous materials. As can be seen from Fig. 5, the hysteresis loop width decreases with functionalization due to the reduction in cavity space. Also, in the isotherm of pure SBA-15, a sharp curve in the capillary condensation regime is observed, which confirms a uniform structure and narrow pore-size distribution of prepared SBA-15. Textural parameters (pore volume, BET surface area and average pore diameter) are displayed in Table 2 for comparison. It can be understood that functionalization reduces the BET surface area and pore volume, which confirms that functional groups of amine have been introduced within the pore of SBA-15 and occupied some free space [43]. Moreover, the decrease in the BET surface area and pore volume can be partly related to the increase in the density of the samples owing to functionalization [44]. The surface area and pore volume of CPX/NH_2-SBA_15 were lower than NH_2-SBA_15, which demonstrated the adsorbed cephalexin were stuck inside the SBA-15 mesopore. The average pore size of SBA-15 was increased after the modification process, which could be described by the grafting of amine functional groups on the small pores of SBA-15. The average particle size of adsorbents was calculated by AFM analyzer (Table 2).

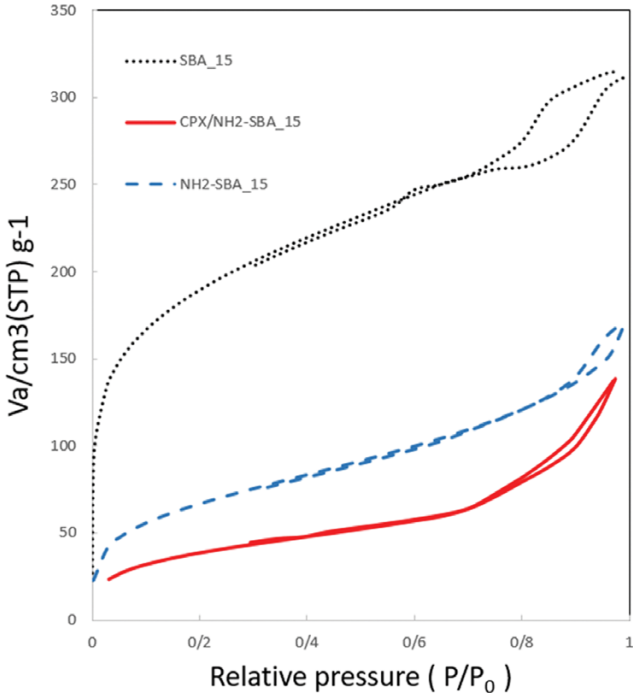


Fig. 5. N2 adsorption and desorption isotherms.

Table 2. The physical properties of the samples

	V_m (cm^3 g^{-1})	$a_{s,BET}$ (m^2 g^{-1})	d (nm)	D^2 (nm)
SBA_15	0.5117	685.2	2.98	400
NH_2-SBA_15	0.2623	247.1	4.24	450
CPX/NH_2-SBA_15	0.1876	144	5.21	500

[2]Average particle size (from AFM analyze)

1-5. Thermal Analysis

Fig. 6 displays TGA and DSC curves of pure SBA_15 silica sample, NH_2-SBA_15 and CPX/NH_2-SBA_15. An understanding of the weight loss requires knowledge of thermally adsorbed species on the surface of SBA-15. The surface of SBA-15 consists of a large amount of silanols and adsorbed water. From the TGA profile of SBA_15, it is clear that the organic content in the structure totally disintegrates at a temperature higher than 700 °C. W1, W2 and W3 represent the first step of the weight loss that could be attributed to physically adsorbed water in pure SBA_15, NH_2-SBA_15, CPX/NH_2-SBA_15, respectively (<100 °C). Our TGA curve shows higher

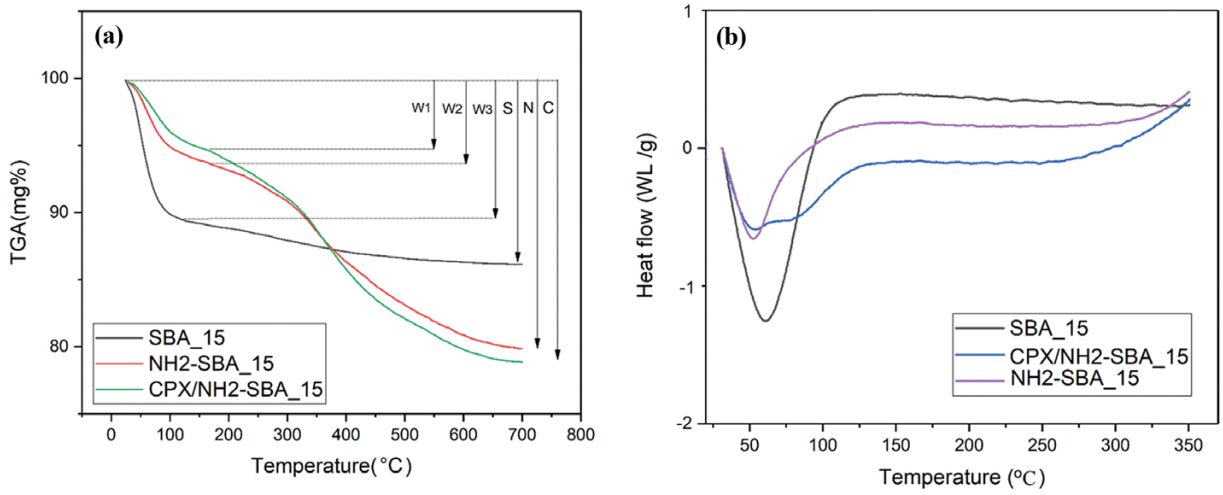


Fig. 6. TGA (a) and DSC (b) profiles of blank SBA_15, NH_2-SBA_15 and CPX/NH_2-SBA_15.

weight loss for pure SBA-15 than functionalized samples (<100 °C). This indicates that the content of adsorbed water of pure SBA-15 (10%) is higher than NH_2-SBA_15 (6.5%) and CPX/NH_2-SBA_15 (5%) due to the absence of functional group, which could hinder the water adsorption by mesostructured. The largest weight loss from the surface dehydration which The DSC profile (Fig. 6(b)) supports this conclusion. S is defined as the percentage weight loss of the adsorbed water and organic part in pure SBA_15 sample. The inflection points at about 300 °C for both samples are mainly assigned to the decomposition of amino groups.

It is clear that application of cephalexin reduced the thermal stability of SBA_15 but increased the number of functional groups on the SBA_15 surface. N shows the percentage total weight loss of adsorbed water, organic part of the hybrid wall structure and APTES group in NH_2-SBA_15 and C is the percentage total weight loss of adsorbed water, organic part of the hybrid wall structure, APTES group and cephalexin loaded in CPX/NH_2-SBA_15 sample. Two endothermic peaks can be seen for CPX/NH_2-SBA_15, which supports this conclusion. In both NH_2-SBA_15 and CPX/NH_2-SBA_15 samples, the organic content to silica ratio must be constant, so the weight percentage of loaded cephalexin (W) in CPX/NH_2-SBA_15 sample can be calculated by the following equation [45]:

$$\frac{N-W2}{100-N}=\frac{C-W1-W}{100-C}$$

The value of W obtained was 2.37%; that is near to the amount calculated in Eq. (1) (2.5%).

As seen in Fig. 6(b), all the studied samples represented the simi-

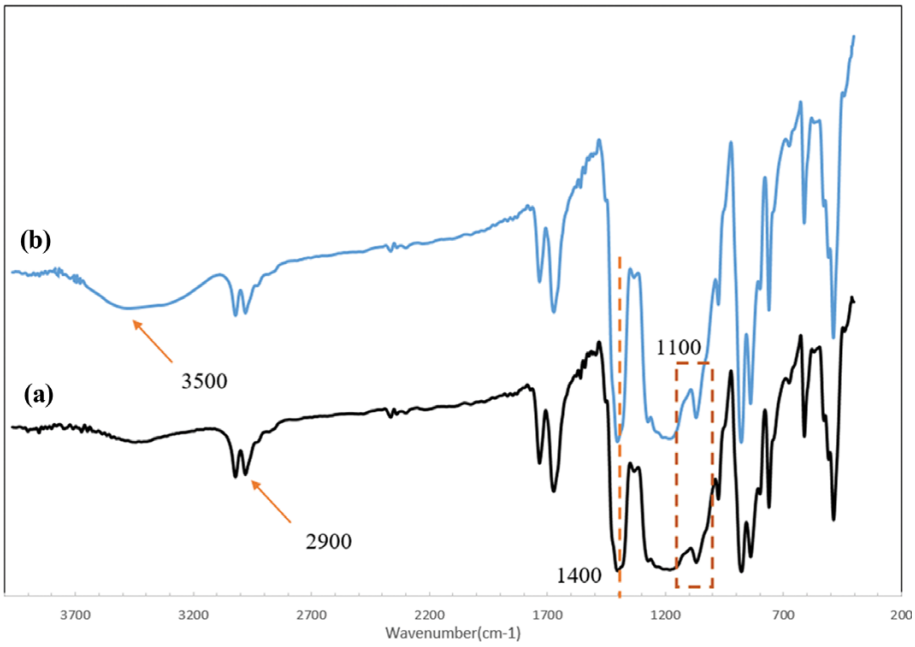


Fig. 7. ATR-FTIR spectra of, (a) pristine PVDF, (b) hydroxylated PVDF.

lar thermal feature. The DSC curves show strong endothermic peaks at temperature below 100 °C, which is related to surface dehydration of absorbed water. After evaporation of water molecules, nanocomposites were thermally stable and no phase transition was observed. A shallow peak occurring for CPX/NH_2-SBA_15 originated because of loss of both components: the grafted APTES and adsorbed CPX molecules [46].

2. Characterization of the Support Membrane

Fig. 7 displays the FT-IR spectra of UF1 and UF2 membranes and provides evidence for functionalization of PVDF. The characteristic vibration peaks of pristine PVDF UF membrane (C-F stretching band and CF_2 groups, 1,100 and 1,400 cm^{-1}; CH_2, 2,900 cm^{-1}; and C=O stretching band, 1,700 cm^{-1}) are observed in Fig. 7(a). Compared to pure PVDF, PVDF-OH membrane obviously shows OH stretching band at peak 3,100-3,600 cm^{-1} (Fig. 7(b)). The existence of hydroxyl broad at 3,000-3,400 cm^{-1} in the FTIR spectrum of PVDF-OH obviously proves successful grafting of the hydroxyl group on PVDF chain [32].

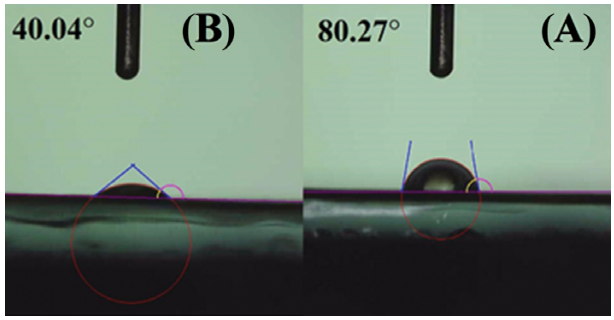


Fig. 8. Contact angle of (A) pristine PVDF, (B) PVDF-OH.

The hydrophilicity of prepared membranes was evaluated by

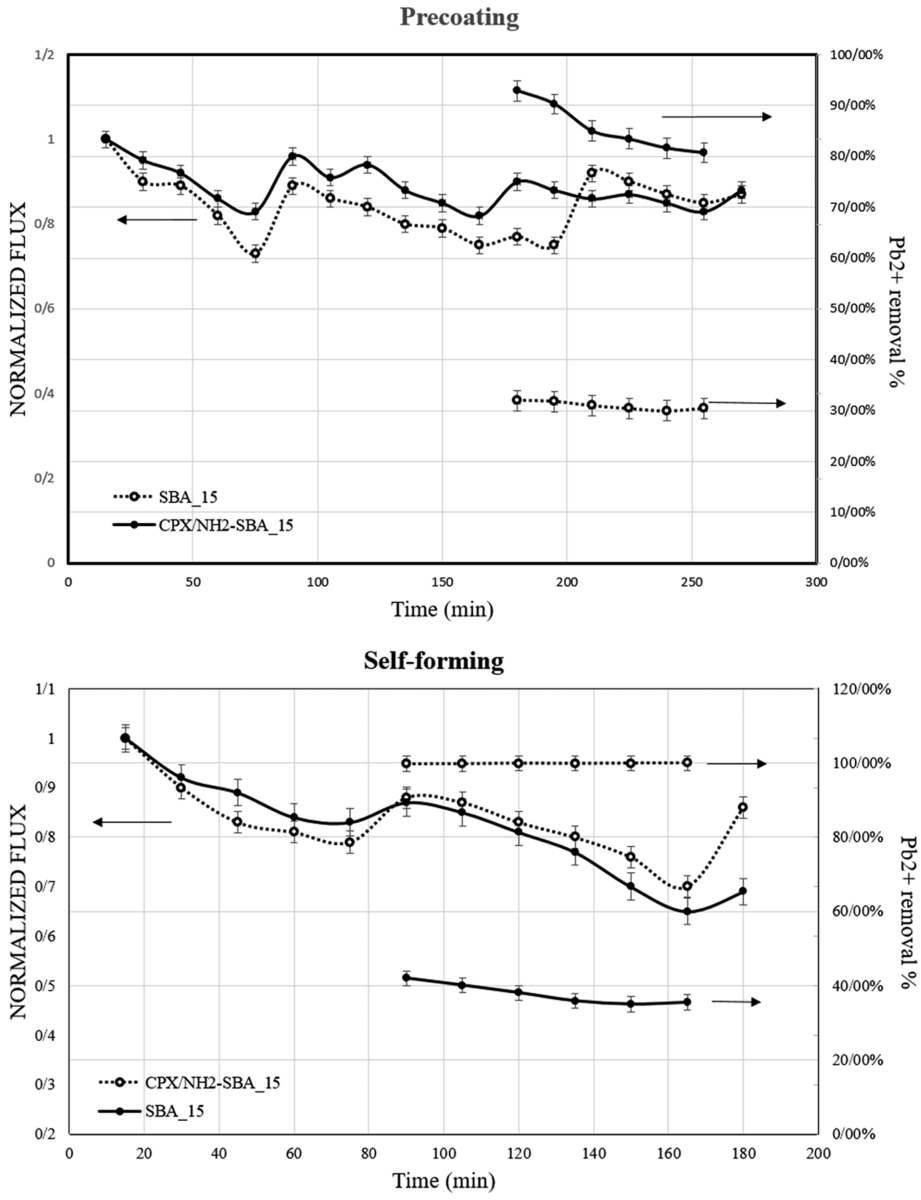


Fig. 9. Normalized flux decline and Pb(II) removal with time during formation of dynamic membranes.

water contact angle measurement (Fig. 8). PVDF-OH membrane with a contact angle of 40.04 was more hydrophilic than that of pristine PVDF membrane (80.27°). It is established that the water permeability is directly related to the membrane hydrophilicity. As regards higher hydrophilicity showing lower fouling potential, PVDF-OH can deeply improve the antifouling performance of polymeric membrane [47]. Average pore size of the support membrane was calculated by AFM analyzer. The average pore size is largely in the range of 370 to 385 nm. The average porosity of support membranes was 47.5% and 55% for PVDF and PVDF-OH membranes, respectively.

3. Dynamic Membrane Performance

The average nanocomposite adsorbent's size was 400-500 nm; that was bigger than the PVDF membrane's pore size, indicating that SBA_15 and CPX/NH_2-SBA_15 can be easily deposited and spread on the support UF membrane's surface as a dynamic layer instead of penetration into the support membrane's pores. On the other hand, the mean size of adsorbent material should not be much larger than the mean pore size of the support UF membrane's surface where adsorbent material can form a uniform dynamic layer with appropriate thickness. Note that the thickness can be controlled by the loading amount of adsorbent material during the formation process.

Fig. 9 shows the normalized permeate flux decline over time during the DMs formation via SBA_15 and CPX/NH_2-SBA_15 as dynamic materials. During the preparation process, the permeate flux remained constant and stable, denoting that the pre-coated dynamic layer had not considerably influenced the permeate flux of the polymeric support membrane. For self-forming DMs, a denser dynamic layer was formed on polymer support membrane by simultaneous filtration of adsorbents and wastewater (in this work aqueous solution of Pb^{2+} ions is unreal wastewater), which was corroborated by the decrease of permeate flux [48]. Further, as shown in Fig. 9, the permeate flux decreased with time during the filtration of the SBA_15 or CPX/NH_2-SBA_15 suspension. The particles accumulated on the surface of polymeric support were compacted by pressure. The dynamic layer was formed after 70 minutes filtration and Pb^{2+} solution was filtered in the next step in pre-coating DM for 100 minutes, and then the pure water flux was measured. The permeate flux decreased sharply in the early of filtration, due to some pore blocking that occurred by the initial deposit layer and cake layer [49]. With precise consideration, the lowest flux was observed during the forming of the SBA_15 suspension, because the smaller size of SBA_15 than that of CPX/NH_2-SBA_15 leads to block the support pores preferably. During formation of pre-coating DM, the permeate flux variation over time was almost repeatable. However, the permeate flux instantly decreased while it began to Pb^{2+} solution filtration again. Also, Fig. 9 shows the permeate flux changes with time by the self-forming method and two dynamic membranes to adsorb and remove the Pb^{2+} (100 ppm) ions. The pure water was filtered 70 minutes at first, then the dynamic layer was formed after 100 minutes filtration and Pb^{2+} removal was calculated, then the pure water flux was measured again. The initial permeate fluxes declined steeply, mainly because of a fast blockage of the support membrane by the particles. It is seen that the normalized flux for SBA_15 DM formation stage decreased almost more due to smaller particles size of the SBA_15 against CPX/NH_2-SBA_15 particles.

As shown in Fig. 9, the dynamic membrane of CPX/NH_2-SBA_15 prepared as self-forming type showed a high Pb^{2+} rejection (more than 99%), so that the obtained Pb^{2+} concentration of the permeate was less than 1 ppm. In the pre-coating type of CPX/NH_2-SBA_15 dynamic membrane, more than 80% was obtained for Pb^{2+} rejection and the Pb^{2+} concentration of permeate was less than 20 ppm. Higher Pb^{2+} rejection of self-forming DMs further proved that a denser dynamic layer was formed on the support membrane surface and contact time between Pb(II) ions and adsorption sites of adsorbent was too long. Also in SBA_15 dynamic membrane, self-forming experiment represented higher Pb^{2+} removal efficiency versus pre-coating manner (Fig. 9). It seems that the higher Pb^{2+} removal of CPX/NH_2-SBA_15 dynamic layer related to SBA_15 is due to more functional groups of the adsorbent surface. This can be defined in terms of the amine groups grafted on the surface of SBA-15 adsorbent, the amino groups in CPX/NH_2-SBA_15 can capture Pb(II) from solution [50].

4. Antibacterial Experiment

The inhibition zone of bacterial growth for pure SBA_15, SBA_15 containing cephalexin and pure cephalexin disks is shown in Fig. 10. Petri dish plate including agar was contaminated with the bacteria. After infection, the disks were deposited on the middle of the solid media, after 24 hour incubation, so that the disks were exposed with the bacteria contaminated surface of the agar. The

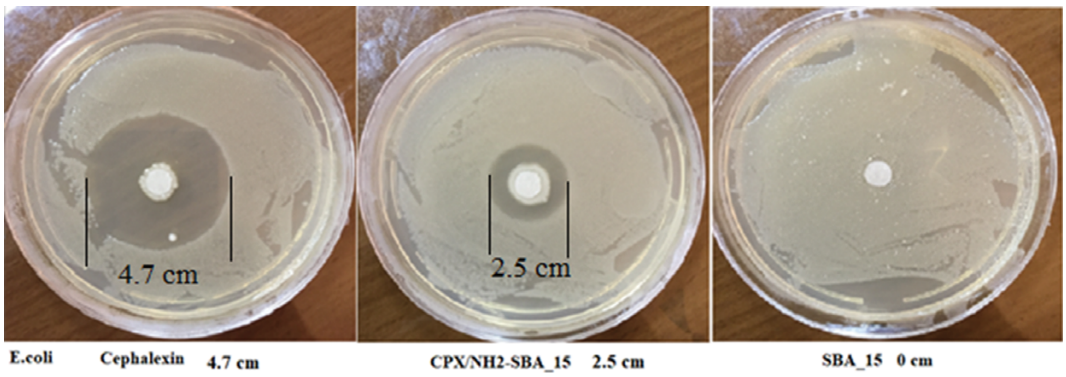


Fig. 10. Inhibition zone areas of different particles.

areas surrounding the cephalexin containing disks are undimmed, which confirms the bacteria could not grow there. This qualitatively represents the bacteriostatic property of the particles. The bacteriostatic effect of cephalexin loaded SBA_15 was clearly seen where microorganism could not grow beside the CPX/NH_2-SBA_15 disks. This test is an acceptable way to the qualitative investigation of adsorbent's antibacterial activity [36]. Photograph of disk diffusion test indicates that the SBA_15 DM membrane did not have anti-bacterial effect. The results show that the CPX/NH_2-SBA_15 composites had significant inhibition capacity toward Gram-negative bacteria where no *E. coli* colonies were observed. The antibacterial activity of the CPX/NH_2-SBA_15 dynamic membranes was mainly caused by the cephalexin particles, not from the SBA_15 nanoparticles.

From the well diffusion method, it can be observed that CPX/NH_2-SBA_15 can give wide zone of clearance against two bacteria. No clearance zone was observed for SBA_15 formulations (Fig. 11). The well diffusion method confirmed the action of CPX/

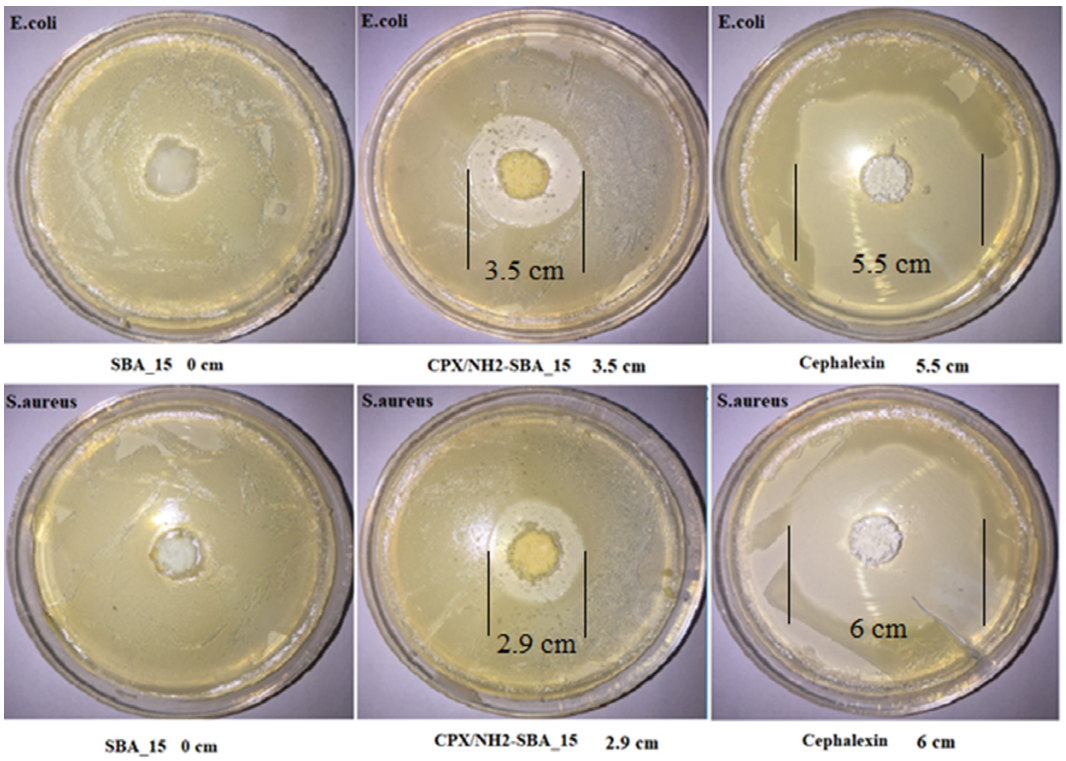


Fig. 11. Well diffusion zones for different particles.

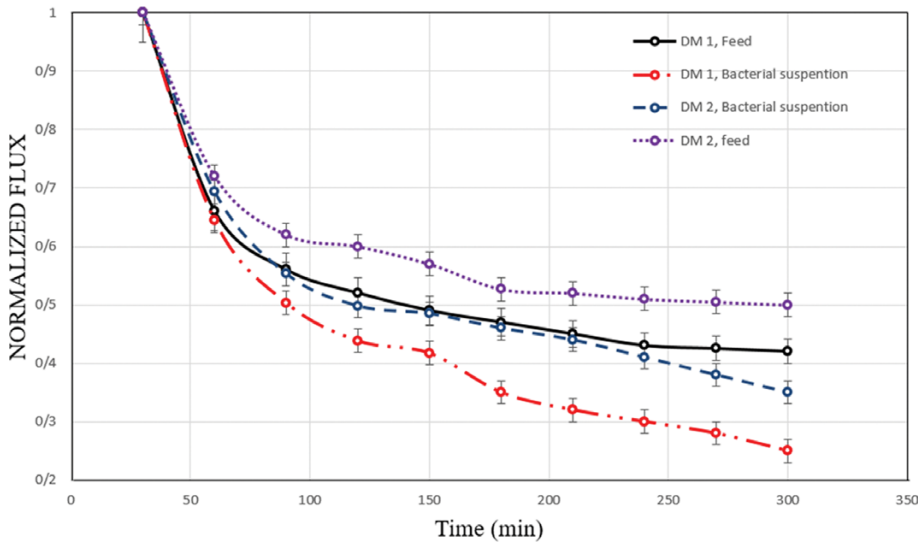


Fig. 12. Normalized flux of filtered concentrated *E. coli* suspension with time.

NH_2-SBA_15 against both bacteria of *E. coli* and *S. aureus*. From the results, it can be seen that the prepared material can effectively diffuse out of the hole into the agar and cause a zone of clearance. Due to the lack of antibacterial properties of SBA_15, it can be concluded the induced antibacterial property was attributed to cephalexin. Wider inhibition zone in well diffusion test than that of disk diffusion test is due to the easy diffusion of cephalexin in agar in well diffusion method versus diffusion from filter paper to agar in disk diffusion method.

From antibacterial tests results, it can be concluded that with the adding of cephalexin, bactericidal (killing of bacteria) and bacteriostatic (inhibition of bacterial growth) activities of the DMs can be gained.

Fig. 12 shows the normalized flux decline of filtered concentrated bacteria suspension and liquid medium with time by different fabricated dynamic membranes. The most biofouling occurred on PVDF support membrane (UF1), which was accordant to its larger pore and hydrophobicity. The hydrophilic mesoporous CPX/NH_2-SBA_15 dynamic layer on the membrane acted as a barrier that hindered the bacteria to get into the support membrane's pore. SBA_15 dynamic membrane indicated lower flux against CPX/NH_2-SBA_15 dynamic membranes, because the existence of microorganisms causes biological fouling in membranes [51]. However, use of cephalexin into the structure of the dynamic layer caused a dramatic decrease in the amount of bacteria and bacterial growth inhibition, so can control biofouling.

Fig. 13 shows a comparison of the flux recovery rate (FRr) of membranes after each filtration cycle. It is the reproducibility of each dynamic membrane after cleaning and washing one time with water, and their flux recovery rate parameters were compared with UF support membrane. The flux recovery rates for CPX/NH_2-SBA_15 pre-coated dynamic membranes, self-forming dynamic membranes and polymeric support were 91%, 87% and 55%, respectively. The filtration conclusions demonstrate that pre-coating CPX/NH_2-SBA_15 DM can be used as a protective membrane to efficiently decrease the fouling of polymeric support membrane. Self-forming CPX/NH_2-SBA_15 DMs had a lower FDr. This phenomenon can be explained by two reasons. First, some amount of Pb^{2+} was adsorbed on adsorbent materials in the suspension before dynamic membrane formation, and second, some amount of metal particles and adsorbent particles were sedimented simultaneously on support membrane surface during the filtration process, thus causing high rejection of lead ions and low flux recovery [52].

CONCLUSION

We have reported the prospering preparation of dual-activity, anti-bacterial and anti-biofouling membranes for heavy metal (Pb^{2+}) removal. Introduction of anti-biofouling properties makes the membranes appropriate for real wastewater and usage. The CPX/NH_2-SBA_15 dynamic membrane could be easily formed using a simple dead-end filtration process. Of course, the permeate flux of the dynamic membranes remained approximately unchanged to that of UF membrane. Therefore, this work highlights the process of dynamic membranes for heavy metal removal. It can be concluded that the DM of CPX/NH_2-SBA_15 as adsorbent with 0.2 gr dynamic layer shows the best performance, high Pb^{2+} rejection and antibacterial activity among these prepared membranes. Owing to the existence of mesoporous silica composite as a protective/separative layer and the presence of the functional group of APTES on SBA_15 surface, the dynamic layer exhibits a higher total removal for Pb(II).

ACKNOWLEDGEMENT

The authors acknowledge the funding support of Babol Noshirvani University of Technology through Grant program No. BNUT/389026/98.

REFERENCES

1. M. Kazemi, M. Jahanshahi and M. Peyravi, *Carbohydr. Polym.*, **198**, 164 (2018).
2. H.-t. Zhao, S. Ma, S.-y. Zheng, S.-w. Han, F.-x. Yao, X.-z. Wang, S.-s. Wang and K. Feng, *J. Hazard. Mater.*, **362**, 206 (2019).
3. S. F. Zakeritabar, M. Jahanshahi and M. Peyravi, *Catal. Lett.*, **148**, 882 (2018).

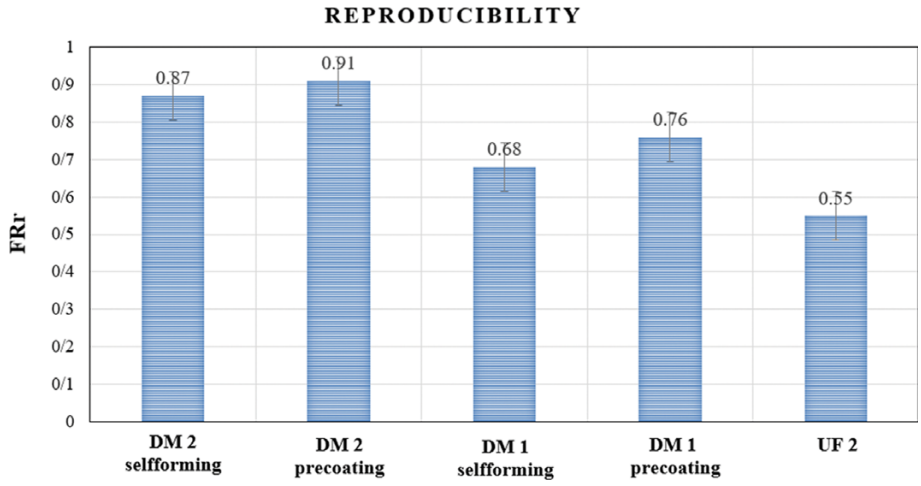


Fig. 13. Flux recovery rate.

4. A. Bera, J. S. Trivedi, S. B. Kumar, A. K. S. Chandel, S. Haldar and S. K. Jewrajka, *J. Hazard. Mater.*, **343**, 86 (2018).
5. A. Rahimpour, M. Jahanshahi and M. Peyravi, *J. Environ. Health Sci. Eng.*, **12**, 55 (2014).
6. Z. Dabaghian, M. Peyravi, M. Jahanshahi and A. S. Rad, *ChemBio-Eng Rev.*, **5**, 119 (2018).
7. E. Dadvar, R. R. Kalantary, H. Ahmad Panahi and M. Peyravi, *J. Chem.*, **7**, 457 (2017).
8. M. Peyravi, M. Jahanshahi, M. Alimoradi and E. Ganjian, *Bioprocess Biosyst. Eng.*, **39**, 1803 (2016).
9. N. Shafaei, M. Jahanshahi, M. Peyravi and Q. Najafpour, *Korean J. Chem. Eng.*, **33**, 2968 (2016).
10. D. Bhagawan, S. Poodari, T. Pothuraju, D. Srinivasulu, G. Shankaraiah, M. Y. Rani, V. Himabindu and S. Vidyavathi, *Environ. Sci. Pollut. Res.*, **21**, 14166 (2014).
11. R. R. Darabi, M. Peyravi, M. Jahanshahi and A. A. Q. Amiri, *Korean J. Chem. Eng.*, **34**, 2311 (2017).
12. M. Khajouei, M. Peyravi and M. Jahanshahi, *J. Membr. Sci. Res.*, **3**, 2 (2017).
13. S. Mansouri, S. Khalili, M. Peyravi, M. Jahanshahi, R. R. Darabi, F. Ardeshiri and A. S. Rad, *Korean J. Chem. Eng.*, **35**, 2256 (2018).
14. M. Peyravi, M. Jahanshahi and S. Khalili, *Chin. J. Chem. Eng.*, **25**, 741 (2017).
15. M. Torkamanzadeh, M. Jahanshahi, M. Peyravi and A. Shokuhi Rad, *Water Sci. Technol.*, **74**, 2737 (2016).
16. O. Isik, A. M. Abdelrahman, H. Ozgun, M. E. Ersahin, I. Demir and I. Koyuncu, *Environ. Sci. Pollut. Res.*, 1 (2019).
17. D. Fazullin, G. Mavrin, I. Shaikhiev and I. Nizameev, *Membr. Membr. Technol.*, **1**, 6 (2019).
18. D. Lu, W. Cheng, T. Zhang, X. Lu, Q. Liu, J. Jiang and J. Ma, *Sep. Purif. Technol.*, **165**, 1 (2016).
19. J. W. Lee, D. L. Cho, W. G. Shim and H. Moon, *Korean J. Chem. Eng.*, **21**, 246 (2004).
20. A. A. Sabri, T. M. Albayati and R. A. Alazawi, *Korean J. Chem. Eng.*, **32**, 1835 (2015).
21. V. Hernández-Morales, R. Nava, Y. Acosta-Silva, S. Macías-Sánchez, J. Pérez-Bueno and B. Pawelec, *Micropor. Mesopor. Mater.*, **160**, 133 (2012).
22. F. Ardeshiri, A. Akbari, M. Peyravi and M. Jahanshahi, *Korean J. Chem. Eng.*, **36**, 255 (2019).
23. P. Pouresmaeel-Selakjani, M. Jahanshahi and M. Peyravi, *Cellulose*, **24**, 1333 (2017).
24. E. Da'na and A. Sayari, *Desalination*, **285**, 62 (2012).
25. C. McManamon, A. M. Burke, J. D. Holmes and M. A. Morris, *J. Colloid Interface Sci.*, **369**, 330 (2012).
26. J. Huang, M. Ye, Y. Qu, L. Chu, R. Chen, Q. He and D. Xu, *J. Colloid Interface Sci.*, **385**, 137 (2012).
27. B. Božić, J. Korać, D. M. Stanković, M. Stanić, M. Romanović, J. B. Pristov, S. Spasić, A. Popović-Bijelić, I. Spasojević and M. Bajčetić, *Free Radic. Biol. Med.*, **129**, 279 (2018).
28. M. Khajouei, M. Jahanshahi and M. Peyravi, *J. Taiwan Inst. Chem. Eng.*, **85**, 237 (2018).
29. M. Cheng, H. Zhao, J. Yang, J. Zhao, L. Yan, H. Song and L. Chou, *Micropor. Mesopor. Mater.*, **266**, 117 (2018).
30. R. Sanz, G. Calleja, A. Arencibia and E. S. Sanz-Perez, *Micropor. Mesopor. Mater.*, **209**, 165 (2015).
31. E. I. Basaldella and M. S. Legnoverde, *J. Solgel. Sci. Technol.*, **56**, 191 (2010).
32. H. Mahdavi, F. Sheikh-Hasani and M. Mahmoudian, *J. Iran. Chem. Soc.*, **13**, 1733 (2016).
33. R. Roshani, F. Ardeshiri, M. Peyravi and M. Jahanshahi, *RSC Adv.*, **8**, 23499 (2018).
34. M. Jahanshahi, M. Peyravi, N. Shafaei and H. Mirani, *Water Sci. Technol.*, **73**, 1 (2016).
35. A. Mollahosseini, A. Rahimpour, M. Jahamshahi, M. Peyravi and M. Khavarpour, *Desalination*, **306**, 41 (2012).
36. Y. Kim, S.-J. Jang, H.-R. Kim and S.-B. Kim, *Korean J. Chem. Eng.*, **34**, 1400 (2017).
37. H. Basri, A. F. Ismail and M. Aziz, *Desalination*, **273**, 72 (2011).
38. S. Hashemikia, N. Hemmatinejad, E. Ahmadi and M. Montazer, *J. Colloid Interface Sci.*, **443**, 105 (2015).
39. A. Shahbazi, H. Younesi and A. Badiei, *Chem. Eng. J.*, **168**, 505 (2011).
40. L. Wang, L. Zhang, H. Li, Y. Ma and R. Zhang, *Compos. B: Eng.*, **156**, 88 (2019).
41. Q. Tao, Z. Xu, J. Wang, F. Liu, H. Wan and S. Zheng, *Micropor. Mesopor. Mater.*, **131**, 177 (2010).
42. Y. Liu, Z. Liu, J. Gao, J. Dai, J. Han, Y. Wang, J. Xie and Y. Yan, *J. Hazard. Mater.*, **186**, 197 (2011).
43. S. J. Mousavi, M. Parvini and M. Ghorbani, *J. Taiwan Inst. Chem. Eng.*, **84**, 123 (2018).
44. S. J. Mousavi, M. Parvini and M. Ghorbani, *Carbohydr. Polym.*, **188**, 197 (2018).
45. C. X. C. Lin, S. Z. Qiao, C. Z. Yu, S. Ismadji and G. Q. M. Lu, *Micropor. Mesopor. Mater.*, **117**, 213 (2009).
46. A. Szewczyk, M. Prokopowicz, W. Sawicki, D. Majda and G. Walker, *Micropor. Mesopor. Mater.*, **274**, 113 (2019).
47. Z. Arif, N. K. Sethy, L. Kumari, P. K. Mishra and B. Verma, *Korean J. Chem. Eng.*, **36**, 1148 (2019).
48. B. Díez, N. Roldán, A. Martín, A. Sotto, J. A. Perdigón-Melón, J. Arsuaga and R. Rosal, *J. Membr. Sci.*, **526**, 252 (2017).
49. Y. Pan, T. Wang, H. Sun and W. Wang, *Sep. Purif. Technol.*, **89**, 78 (2012).
50. K. Alizadeh, E. Khaledyan and Y. Mansourpanah, *J. Water Environ. Nanotechnol.*, **3**, 243 (2018).
51. A. B. Rostam, M. Peyravi, M. Ghorbani and M. Jahanshahi, *Appl. Surf. Sci.*, **427**, 17 (2018).
52. M. Saleem, A. Spagni, L. Alibardi, A. Bertucco and M. C. Lavagnolo, *J. Environ. Manage.*, **213**, 27 (2018).